Revista Brasileira de Física, Vol. **8,** N? **1, 1978**

Magnetic Hysteresis and Flux Profiles in Type-I Superconductors

GUNTER ZERWECK

Instituto de Física "Gleb Wataghin", Universidade Estadual de Campinas*, Campinas SP

Recebido em 23 de Novembro de **1977**

Dedicated to the memory of Dr. Herman Trauble

The critical current of type-I superconductors is determined by the interaction of quantized magnetic flux lines with inhomogeneities ("pinning"). Measurements of the profiles of the magnetic induction are equivalent, in many respects, to critical current rneasurements, and frequently are much simpler. After a short introduction about the general properties of type-I superconductors, this article reviews the main microscopic pinning mechanisms, their statistic cooperation to the macroscopic volume pinning force, and the generalized critical state model including surface effects. The basic methods of measurement are described, together with some important results about bulk, surface, and near-surface pinning. The final discussion stresses especially two observations still hardly understood: the different effects of the surface and the influence of magnetic field history.

A corrente critica de supercondutores de tipo-II é determinada pela interação de linhas quantizadas de fluxo magnético com inomogeneidades ("pinning", aprisionamento). Medidas de perfis da indução magnética são equivalentes, em muitos aspectos, a medidas da corrente critica, e frequentemente bem mais simples. Após uma introdução curta sobre as propriedades gerais de supercondutores de tipo-II, este artigo apresenta uma resenha dos mecanismos microscópicos de aprisionamento mais importantes, a cooperação estatística deles à força macroscópica por volume, e o modelo do estado critico generalizado, incluindo efeitos da super-

* Posta! Address: C.P. 1170, 13.100 - Campinas SP

fície. Descrevem-se os métodos básicos da medida, e alguns resultados importantes sobre aprisionamento no volume, na superfície e nas proximidades da superfície. A discussão final acentua especialmente duas observações ainda pouco entendidas: os diferentes efeitos de superfície e a influência da história do campo magnético.

INTRODUCTION

Application of superconductivity began in 1961 when Kunzler et *al.* discovered[13] that the compound Nb_3Sn is able to carry a high current without destroying superconductivity. Since then, highly sophisticated conductors have been developed, mainly for the production of magnet coils for a wide range of applications, ranging from the laboratory magnets for basic research purpose to the levitating magnets in high-speed train systems[6,14]. Another field where superconductivity may become of increasing practical interest is the transmission of electric power in cryogenic cables, a project which is presently being studied in a number of laboratories all over the world (see, e.g., Ref.15). A survey of the actual state of application of superconductivity was published recently by Schwartz and Foner[7].

All these devices make use of the ability of type-II superconductors to carry a lossless current up to a certain critical current I_c. This critical current is a function of temperature and magnetic field, and is mainly determined by the interaction of magnetic flux vortices with extended crystal imperfections like precipitates, dislocation walls, or grain boundaries. A transport current creates a force on the vortices, and to keep them from moving, which would cause power dissipation, they must be "pinned". The stronger the interaction between defects and flux vortices, the higher the critical current. On the other hand, the critical current of an "ideal" type-II superconductor (single crystal without any defects) in the mixed state would be zero, even in materials with high critical temperature and high critical fields.

The same interaction prevents, in magnetization experiments, the flux vortices from reaching their thermodynamic equilibrium distribution, thus al-

lowing for the presence of flux gradients within a bulk superconductor, and giving rise to a hysteretic magnetization curve.

This equivalence between a transport current and a flux density gradient, in type-II superconductors, is the basis for the experimental study of "pinning" forces in model systems by magnetization measurements. Such model systems, each of which ideally represents only a single interaction mechanism, instead of the metallurgically complicated state of the technical superconductor, are, e.g., single crystals with one defect type: dislocations, irradiation defects, or precipitates. Because of the high critical currents (up to $10^6 A/cm^2$), sample preparation for magnetization measurements (long cylindrical rods) is much easier in such systems than for direct current-voltage measurements (thin tapes or threads). The purpose of the present article is to describe how much information about pinning forces can be drawn from magnetization measurements, especially from the so called "minor hysteresis loops". We do not intend to present a complete review of irreversible properties of type-II superconductors. This was excellently done by Campbell and Evetts[8] and, more recently, by Ullmaier[9]. Both reviews also contain a more comprehensive bibliography. Detailed information about many specific problems may be obtained from the proceedings of the discussion meeting in St. Andreasberg in 1974, Ref. 10. Melville's review paper[11] stresses the great influence of the surface on a.c. losses, which are closely related to the magnetization hysteresis treated in the present paper. The article of Livingston and Schadler[12], although 13 years old, may still serve as a valuable introduction to the whole field of relations between superconductivity and metallurgy.

In Section 1, a short introduction to the general properties of type-II superconductors is presented. The second Section describes, in a qualitative rather than in a mathematically exact way, the main microscopic interaction mechanisms and the statistic summation of these elementary forces to the macroscopic volume pinning force. One of the most fruitful ideas for the understanding of irreversible effects in type-II superconductors was the concept of the critical state, introduced by Bean[16], which will be treated in Section 3, followed by a review of different methods of measurement. The last two Sections present some important experimental results about bulk and surface pinning, and discuss

specially the different effects of surface and near-surface pinning as well as the influence of magnetic field history.

1. TYPE-II SUPERCONDUCTORS

This Section is just to give a concise introduction to the equilibrium properties of type-II superconductors and the basic phenomenological concepts for describing them. For more details, I must refer to one of the textbooks listed in the first part of the bibliography[1-5].

The difference between type-I and type-II superconductors is best illustrated by theirequilibriumrelation betweenmagnetic induction (flux density) B and the applied field H (Figs. 1a and 1b). Type-I superconductors are charaterized by a complete exclusion of the magnetic flux (perfect diamagnetism) up to the critical field H_c, where the transition to the normal state takes place. In type-II superconductors, the surface energy between superconducting and normal phases is negative, thus the free energy can be decreased, in fields above the lower critical field H_{c1}, by a splitting into normal and superconducting "domains" on a very fine scale. This is accomplished by a partial penetration of magnetic flux, reflected by that part of the B–H curve of Fig.1b between H_{c1} and H_{c2} ("mixed state"). At the upper critical field H_{c2}, the flux penetration is complete and the bulk of the specimen becomes normal.

For practical reasons (higher resolution of the ordinate), the magnetization curve $-M(H)$ is given instead of the induction curve $B(H)$ in most cases (Fig.1c). The magnetization M may be defined by

$$B = \mu_0 \cdot (H + M) \ , \qquad (1.1)$$

although it does not have the direct physical meaning of a magnetic dipole density as, e.g., in ferromagnets. With this definition, the initial slope of the magnetization curve in the perfectly diamagnetic state becomes -1.

A theoretical description of this behavior is provided by the Ginzburg-Landau equations[17], twa coupled nonlinear differential equations for the

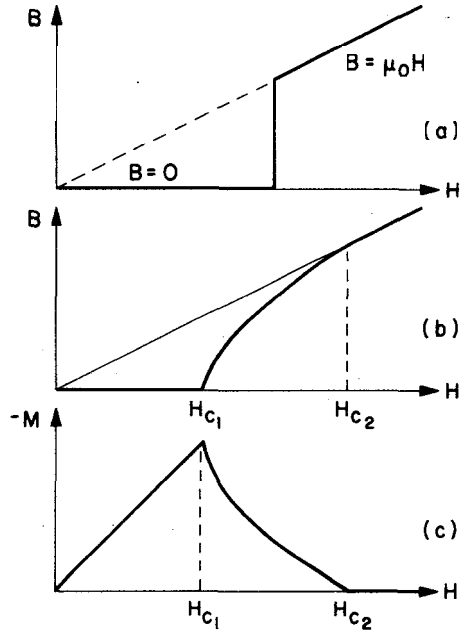

Fig.1 - Equilibrium induction vs. field, and magnetization curves of superconductors: a) type-I superconductors, b) type-II superconductors, c) magnetization curve of a type-II superconductor.

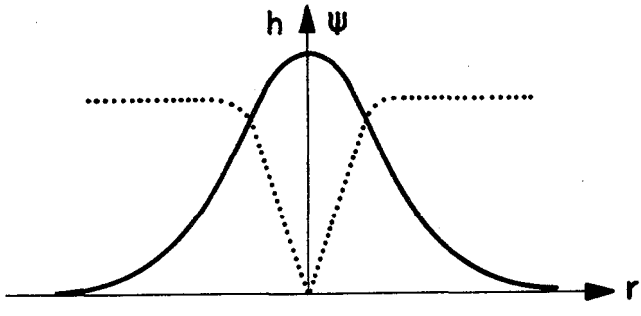

Fig.2 - Structure of a single vortex line (solid line: microscopic magnetic field h; dotted line: order parameter ψ).

order parameter ψ which might be interpreted as a kind of macroscopic wave function for the condensed electrons, and for the vector potential $\vec{A}$. They contain two material parameters with the dimension of a length, i.e., λ ("penetration depth") and ξ ("range of coherence"), which represent the characteristic lengths of variation of the microscopic field h and of the order parameter ψ, respectively. Typical values of λ and ξ are of the order of some hundred Angstroms.

The ratio λ/ξ is the dirnensionless Ginsburg-Landau parameter κ. In type-II superconductors, $\kappa > 1/\sqrt{2}$. The ratio of the critical fields H_{c2}/H_{c1} increases monotonically (but not linearly) with κ. The two characteristic lengths and the Ginsburg-Landau parameter vary strongly with the mean free path of the normal electrons. In a certain alloy system, the parameter κ increases linearly with the residual resistivity[18]. Therefore, alloys generally are type-II superconductors with $\kappa > 1/\sqrt{2}$.

In 1957, Abrikosov[19] found periodic solutions of the Ginsburg-Landau equations which only severa1 years later were recognized as describing exactly the mixed state of type-II superconductors[18]. Abrikosov's solution showed that the mixed state consists of a two-dimensional array of vortices or flux lines each of which carries one flux quantum ϕ_0:

$$\phi_0 = h/2e = 2.07 \times 10^{-15} \text{ V.s} = 2.07 \times 10^{-7} \text{ G.cm}^2. \qquad (1.2)$$

Each flux line can be imagined to consist of a normal conducting core with a maximum of the microscopic magnetic field $\vec{h} = \text{curl } \vec{A}$, surrounded by circulating supercurrents (Fig.2).

In an ideal (reversible) type-II superconductor, these vortices form a regular two-dimensional lattice, usually of hexagonal symmetry. The experimental observation of this regular lattice (Fig.3), first by neutron diffraction[20] and later directly by a decoration technique[21,22], was the proof for the correcteness of Abrikosov's solutions. The rnagnetic structure of a single flux line within the lattice was also studied by a precise determination of the form factor in neutron diffraction[23].

Because each vortex contains one quantum of magnetic flux, ϕ_0, the mean flux density $B = \langle h \rangle$ is related to the line density n of the vortices

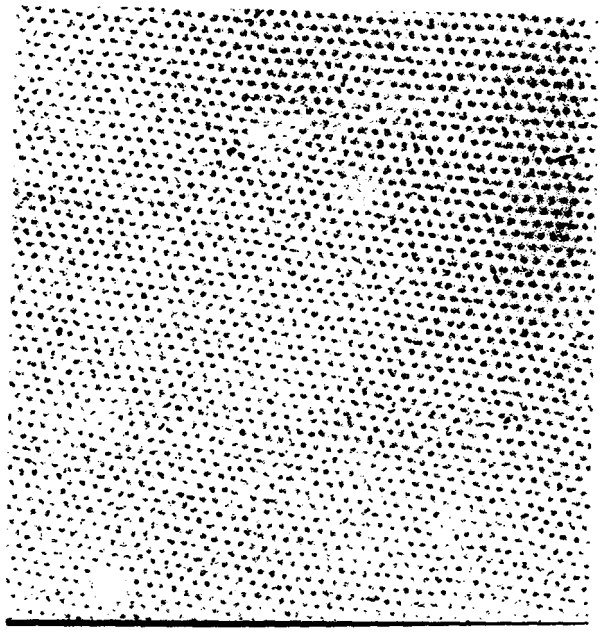

Fig.3 - Perfect triangular flux line lattice (FLL) as emerging from the top face of a superconducting niobium cylinder ($B = 73\ mT$). The points of exit of the flux lines are decorated by small ferromagnetic particles (photograph by U. Essmann).

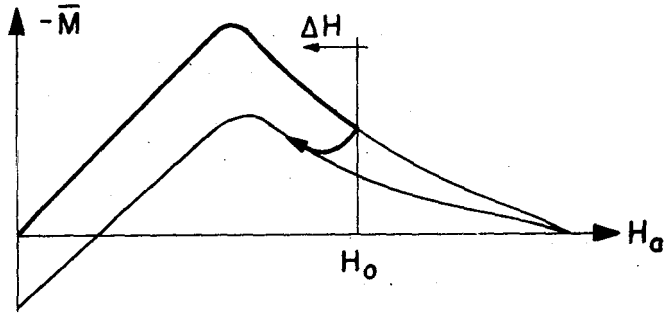

Fig.4 - Irreversible magnetization curve with minor hysteresis loop.

by $B = n.\phi_0$. In thermodynamic equilibrium, the line density n, and thus the induction B, is constant throughout the sample, and at a certain temperature a unique function of the applied field H (Fig.1b): $B = B_0(H)$.

Although the lattice parameter of the flux line lattice (FLL) is several orders of magnitude greater than that of crystal lattices (several thousand Angstroms), there are many analogies between them. The FLL is elastically deformable, and can be described by tensors of elastic strain and stress[24,26], and elastic constants connecting them[27,31]. However, because of the long-range interaction between the flux lines, the elasticity theory of the FLL is highly non-local. This has important consequences for strains and stresses varying at short distances[32,33] but was not considered until quite recently (Refs.24,25,34). Another analogy between FLL and a crystal lattice is the existence of lattice defects (vacant lines, interstitials, dislocations, stacking faults[35,36]) which in som cases may strongly influence flux movement and the critica1 current[37-41].

2. PINNING FORCES

In thermodynamic equilibrium, the line density n of the vortices is constant throughout the sample, a state which can only be realized if the vortices are freely movable. In real crystals, however, there are always inhomogeneities with spatial variations of the free energy for a vortex which give rise to attractive or repulsive interaction potentials and forces. The maximum effective interaction force, f_m, between one flux line and one defect is called "elementary pinning force". In the following, the main interaction mechanisms in the bulk and at the surface of the specimen are described in a qualitative way. More details and quantitative formulations can be found in the original papers we referred to, and in the two review articles of Refs. 8 and 9.

2.1. Pinning Interactions in the Bulk

The specific volume of a metal increases by about 10^{-7} at the transition to the superconducting state. Thus the core of a vortex is a contracted cylinder within a superconducting matrix. This effect is further accen-

tuated by the magnetostriction caused by the microscopic field $\vec{h}$ around each vortex. Thus each flux line, especially the core but also the region of decreasing field, is a source of eigen-stresses[42] which interact with the stress field of a lattice defect. This first-order interaction (Δ-V effect, para- elastic interaction) was first described by Kramer and Bauer[43] and further studied, for specific defects, by Kronmüller and Schmucker[44,45].

A second-order elastic interaction is due to the softening of the crystal lattice in the transition to the superconducting state. The relative decrease of the elastic constants is of the order of 10^{-4}. The elastic self-energy of a lattice defect depends on the elastic constants, thus it is higher in and near the core of a flux line. A first estimate of this repulsive interaction (A-E effect, dielastic interaction) between a screw dislocation and a simplified flux line was published by Webb[46]; a very general treatment based on Seeger's and KronmÜller's micromagnetic equations of superconductors[47,48] was recently given by Schneider[49,50].

A third, non-elastic, interaction is caused by spatial variations of superconducting material parameters like the Ginzburg-Landau parameter κ (hence A-K effect) in precipitates or clusters of defects. The self-energy of a vortex line can be decreased, for example, by passing partly through a normal conducting precipitate or a void. A similar mechanism acts in a grain boundary: because of the anisotropy of material parameters like H_{c2} (Ref.51) and thus of the Ginzburg-Landau parameter κ, the self-energy of the vortex may be different in two adjacent grains, thus leading to pinning effects due to the grain boundary.

A general feature of all these pinning mechanisms is that they are only effective if, loosely speaking, the dimensions of the defects are at least of the order of the core diameter, i.e. some hundred Angstroms. Thus, defects like vacancies or non-magnetic impurity atoms can only pin weakly through their eventual density fluctuations, whereas a homogeneous distribution does not give rise to any pinning effect.

2.2. Statistic Summation

A comparison of the observed mean volume pinning forces, p_v, with these elementary pinning forces revealed that the former were frequently one order of magnitude smaller than expected from a simple summation of the elementary f_m forces. This is due to the elastic coupling of the vortices within the FLL which allows only a small fraction of the pinning sites to act with the maximal force f_m. A consideration of the two limiting cases of a completely rigid and a completely soft FLL will clarify this argument: If the FLL is completely rigid and if there is a statistical distribution of pinning sites, there will be an equal number of sites acting with force $\vec{f}_m$, and with force $-\vec{f}_m$, thus the net pinning force on a rigid FLL will be zero. In a completely soft lattice, on the other hand, the vortices can occupy the positions of maximum force f_m at all pinning sites, thus for a density N_p of the pinning centers, the mean volume pinning force will be $N_p \cdot f_m$. The intermediate case, however, the statistic summation of the pinning forces in an elastic FLL, is a rather complicated problem, and its detailed description is far beyond the scope of this article. The first approach to a solution of this problem was made by Yamafuji and Irie[52,53], who considered the energy dissipated during flux movements (dynamic approach). The statistical treatment of the static FLL in the critical state was elaborated by Labusch[54]. For statistically distributed point pinning centers, both theories yield, for the mean volume pinning force, the expression

$$p_v = a \cdot N_p \cdot f_m \cdot (B/\phi_0) \cdot S(0) \quad , \tag{2.1}$$

where a is the radius of the pinning centers of density N_p, B the magnetic induction, ϕ_0 the flux quantum, and $S(0)$ the maximum displacement of the flux at the pinning center. The local theory of elasticity of the FLL gives for this displacement[28]

$$S(0) = \frac{1}{4\sqrt{\pi}} \cdot \frac{B}{\phi_0} \cdot \frac{f_m}{C_{eff}} \quad , \tag{2.2}$$

where C_{eff} is an effective elastic constant given by

$$C_{eff}^{-1} = (C_{11} C_{44})^{-0.5} + (C_{66} C_{44})^{-0.5} \quad . \tag{2.3}$$

Recent calculations, based on the nonlocal elastic properties of the flux line lattice, showed that the displacement may be larger by a factor of up to 100 depending on the flux density B, the relation between $S(0)$ and f_m, however, remaining linear[33].

A different approach which may be more appropriate for the case of high defect densities was made by Kornfeld and Kronmüller[55] using the concept of "flux bundles" [56], and further elaborated by Schmucker and Kronmüller[44,45] for pinning by density fluctuations of point defects and by dislocations.

2.3. Surface Pinning

In contrast to these pinning mechanisms in the interior of the material, the effects of the surface are not yet so well established. At verysmooth surfaces parallel to the vortices, there exists a barrier against entry and exit of vortices resulting from the distortion of the vortices necessary to obey the boundary condition of zero normal current. This distortion can be interpreted as arising from "image vortices" outside the specimen, and the barrier as being due to an attractive interaction between the real and the image vortices[57,58]. Roughening of the surface will decrease this barrier. Experimentally, however, it was frequently observed (see Section 5) that surface pinning increased when the surface was roughened[59,60]. Thus also geometric irregularities of the surface, like asperities or slip lines, for example, must be considered pinning centers.

Another effect of the surface is the reduction of the coupling of the flux lines to the FLL which can be described as a softening of the FLL in a surface layer. Extending Brandt's oalculations of the elastic constants[29], to the case of a plane surface separating a semispace with a real flux line lattice from another with an image lattice[63], it is possible to estimate that C_{66} is the elastic constant with the strongest decrease in a surface layer of 10 to 20 lattice constants (Appendix A). As the effective elastic constant C_{eff} in Eq.(2.2) is mainly determined by C_{66}, pinning centers like dislocations or precipitates will bemuch more effective in this surface layer than in the bulk of the material[6@].

There is no theory yet for the statistic summation of these elementary surface and near-surface interactions. Because of the softening of the FLL in the surface layer, however, it is expected that the naive suma-tion of the elementary surface forces should give a rather good valw for the observable mean surface pinning force p_s.

3. THE CRITICAL STATE

The phenomenological model of the critica1 state describes irreversible effects in superconductors using macroscopic concepts like the "flux density gradient" and the "mean volume pinning force", without considering the details of the underlying mechanisms. The relation between microscopic and macroscopic description of pinning effects can be illustrated by the example of a sand hill: although the elementary frictional interaction between single sand grains may be rather complicated, the knowledge of one macroscopic quantity, the maximum possible inclination of the slope ("critica1 slope"), is sufficient to predict macroscopic properties of a sand hill. In a similar way, the cooperation of the elementary pinning interactions gives rise to the existence of a certain "critical flux density gradient", the niaximum gradient which can be maintained by a certain distribution of pinning centers. For a quantitative elaboration of the mdel, the elastic properties of the flux line lattice are essential.

The local equilibrium condition for an elastic continuum in the presence of a volume force $\vec{p}_v$ can be written as

$$\operatorname{div} \sigma + \vec{p}_v = 0 \ , \tag{3.1}$$

or, in components,

$$\sum_i \frac{\partial \sigma_{ij}}{\partial x_i} + p_{v,j} = 0 \ , \tag{3.2}$$

where a is the (second order) elastic stress tensor which, in linear elasticity theory, is related to the strain tensor ε by Hooke's law. For a triangular flux line lattice, the tensor C of the elastic constants has three independent components (e.g., C_{11}, C_{44} and C_{66} in Voigt's notation) which have been calculated by several authors (Refs. 27-31, 34).

In magnetization experiments, a two-dimensional isotropic compression normal to the vortices is the most important elastic deformation, the "bulk modulus" C_L being given by

$$C_L = C_{11} - C_{66} = B_0^2 \cdot \left(\frac{\partial B}{\partial H}\right)_0^{-1} \quad . \tag{3.2}$$

The index 0 is to denote local equilibrium, $(\partial B/\partial H)_0$ being the slope of the reversible inductions vs. field curve. For this type of deformation, the components (11) and (22) of the stress and strain tensors are equal, and all the others are zero. The trace of the strain tensor ε (the relative size change of an area S normal to the vortices) is related to the difference ΔB of the flux density B from its equilibrium value B_0 by

$$\Delta S/S = \mathrm{tr}\ \varepsilon = -\Delta B/B_0 \quad . \tag{3.3}$$

Thus Hooke's law yields, for the nonzero components of the stress, the expression

$$\sigma_{11} = \sigma_{22} = C_L \cdot \mathrm{tr}\ \varepsilon = -B_0 \cdot (\partial B/\partial H)_0^{-1} \cdot \Delta B \quad . \tag{3.4}$$

If now ΔB and thus the deformation varies in a direction normal to the vortices, Eq. (3.1) yields the necessary volume force $\vec{p}_v$ which must be provided by the pinning centers to keep the system in equilibrium:

$$\vec{p}_v = B_0 \cdot (\partial B/\partial H)_0^{-1} \cdot \mathrm{grad},\ \Delta B = B_0 \cdot (\partial B/\partial H)_0^{-1} \cdot \mathrm{grad},\ B \quad , \tag{3.5}$$

where the symbol grad_2 stands for the two-dimensional gradient in the x-y plane normal to the vortices. This equationwas first derived by Friedel et $al.$[65] using thermodynamic arguments, and therefore the expression on the righthand side is sometimes called Friedel force.

Eq. (3.5) is a special form, for isotropic compression varying normally to the vortices, of the more general equation[66]

$$\vec{p}_v = \vec{B} \times \mathrm{curl}\ \vec{H} \quad , \tag{3.6}$$

which may be interpreted as follows. A current density $\vec{j} = \mathrm{curl}\ \vec{H}$ acts

on the system of vortices (of mean flux density $\vec{B}$) with the "Lorentz force" $\vec{p}_L$

$$\vec{p}_L = \vec{j} \times \vec{B} \quad . \tag{3.7}$$

Thus, Eq. (3.6) is the condition that, in equilibrium, the sum of Lorentz force and mean volume pinning force is zero.

These considerations give the quantitative basis for the far reaching equivalence between the magnetic hysteresis and the critical current of a type-II superconductor. However, whereas in magnetization experiments a real flux density gradient is realized (Eq.3.5), the deformation of the FLL in critica1 current measurements is much more complicated (in general the flux lines are curved[6] which demands the use of the more general Eq.(3.6)).

If the flux density B varies continuously within the specimen, Eq. (3.5) yields the necessary volume pinning force to maintain this flux density gradient which is equivalent to a bulk current density. If, on the other hand, the limiting flux density B_s at the specimen surface is not in equilibrium with the applied field H_a, there is a discontinuous jump $\Delta B_s = B_s - B_0(H_a)$ of the flux density (equivalent to a surface current perlength of the specimen) which can only be maintained by a surface pinning force $\vec{p}_s$. By integrating Eq.(3.5), one obtains

$$p_s = B_0 . (\partial B/\partial H)_0^{-1} \; . \; \Delta B_s \quad . \tag{3.8}$$

For a given distribution of pinning centers, there is a certain maximum value of the volume and surface pinning forces, p_{vm} and p_{sm}, which are determined by the density and type of the defects, and which in general will be a local function of the flux density and temperature. It should not, however, depend explicitly on further variables such as the magnetic history, the sign of the gradient, the distance from the surface, the flux density in neighbouring points, etc. In Section 5, we shall see how far these assumptions could be confirmed experimentally.

A consequence of the existence of a maximum volume and surface pinning forces is the *critical* state. It is defined as that state in which the

flux density gradient, $\mathrm{grad}_2 B$, and the flux density jump at the surface, ΔB_s, take their maximum possible values (a and ΔB_s^c). These values are determined by p_{vm} and p_{sm} together with Eqs. (3.5) and (3.8). The importance of the critical state, a concept introduced by Bean[16], is based on the fact that in most experiments $\mathrm{grad}_2 B$ and ΔB_s adjust and maintain themselves always to a and ΔB_s^c. Thus, the measurement of these quantities gives directly the *maximum* volume and surface pinning forces.

Let us consider, e.g., an isothermal magnetization process of a long cylindrical sample without surface pinning, but with bulk pinning centers, in a parallel field. When the applied field is increased above H_{c1}, flux lines will be nucleated at the surface of the sample. The situation is unstable, with consequent movement of the lines into the interior, as long as the flux density gradient is greater than a. Upon reaching the critical gradient, however, the vortices will stop moving and the situation will become stable. A further increase of the applied field again will cause a movement of the vortices until a new critical state is established. Decreasing the magnetic field causes the flux density gradient to adjust itself again to its critical value, this time with opposite sign. Thus in the critica1 state

$$\mathrm{grad}_2 B = \pm \alpha(B,T) \quad , \tag{3.9}$$

where the upper and lower signs correspond to an increasing and a decreasing field, respectively.

In the absence of surface pinning, the flux density B_s at the surface is in equilibrium with the applied field H_a; with surface pinning, B_s in the critical state takes the value

$$B_s^c = B_0(H_a) \mp \Delta B_s^c(B,T) \quad , \tag{3.10}$$

with the same sign convention as for Eq. (3.9). Thus the flux density profile is completely determined by these two equations. The local flux density is lower than the equilibrium value $B_0(H_a)$ at all points in the interior of the specimen inan increasing field, and higher in a decreasing field, thus leading to a hysteretic $\bar{B}(H_a)$ curve.

As the critical state is not a state of thermdynarnic equilibrium, it cannot be completely stable. Anderson[56] was the first to propose a thermally activated "flux creep" in the critical state toward thermodynamic equilibrium ($B=B_0$). Later, this effect was experimentally observed, e.g. in one of the few quantitative measurements by Antesberger and Ullmaier[68]. The observed creep rates, however, are so low (a typical relative change of the flux density gradient is of the order of 10^{-3} per hour, Refs.9 and 69) that the static critical state model is sufficient for mst practical purposes. This flux creep should not be confused with "flux flow", the movement of vortices caused by overcritical flux density gradients or overcritical currents.

The critical state mdel, as described so far, cannot be complete in another sense, to ~ for geometric reasons, a flux density gradient normal to the vortices can only be created without macroscopic lattice curvature by distributing dislocations in the FLL[35]. A simple geometric relation between the density of flux line dislocations and the flux density gradient was deduced and experimentally proved by Essmann and Träuble[70,36]. The critical state may be influenced by the presence of these dislocations, either by the violation of local equilibrium in their neighbourhood or by their influence on the critical shear stress of the FLL[8,38]. Recently, Schmucker[39,41] treated quantitatívely the effect of flux line dislocations on the statics (Eq.3.5) and dynamics of a pinned FLL.

4. MEASUREMENT OF FLUX PROFILES

The only direct method of measuring elementary pinning forces f_m is provided by neutron diffräction[71] since the width of the so called rocking curves is directly related to the mean bending of the vortices. In general, however, the determination of pinning forces in magnetized specimens is based on measurements of flux profiles which, by Eqs. (3.5) and (3.8), are related to the mean volume and surface pinning forces p_v and p_s.

The hysteretic $\bar{B}(H)$ and rnagnetization curves reflect only mean properties over the whole specimen cross section (the same is valid for the mecha-

nical measurements, s. Ref.72). This integrated information can only be analized quantitatively in terms of pinning forces for specimens with very small dimensions in the direction of the gradient[68,73], and without surface pinning, so that the flux density gradient can be considered constant across the sample in a good approximation.

4.1. Minor Hysteresis Loops

The method of "minor hysteresis loops" offers the possibility of measuring separately volume and surface pinning forces as a function of the local flux density in bulk cylindrical sarnples. It was developed by severa1 authors for different measurement techniques. In the so-called d.c. techniques, the applied field is varied linearly in time, and the corresponding variation of the magnetization[74,75] or the differential susceptibility[60,76] is measured. The same information is obtained from a.c. techniques, where a small a.c. field is superimposed on a large d.c. field. The voltage signal induced in a pick-up coil can be analized harmonically[77,78], directly from its waveform[79,80], or by integration using a lock-in amplifier[81]. All these methods of minor hysteresis loops are based on the generalized concept of critica1 state described in the preceding Section. As an example, the technique of differential susceptibility measurement will be described in more detail since this technique gives a direct graph of the flux density profile. The experimental arrangement consists of a pick-up coil wound closely on a long cylindrical specimen, and a compensation coi1 witl the same product (turns.area), but at a certain distance from the specimen. The two coils are adjusted to give a total voltage signal, u, which is proportional to the time variation of the mean magnetization

$$u \propto \frac{d\bar{M}}{dt} = (1/\mu_0)\,\frac{d\bar{B}}{dt} - \frac{dH}{dt} \,. \qquad (4.1)$$

If the applied field H_a varies linearly in time, this voltage is proportional to the differential susceptibility χ,

$$\frac{d\bar{M}}{dt} = \frac{d\bar{M}}{dH} \cdot \frac{dH}{dt} = \chi \cdot \frac{dH}{dt} \,. \qquad (4.2)$$

Fig.4 shows schematically a hysteretic magnetization curve of a type-II superconductor. The applied field is at first monotonously increased to the

value H_0, and then decreased with a constant sweep rate dH/dt. The mean magnetization follows the bold curve connecting the two branches of the hysteretic magnetization curve. The resultant induced voltage signal of the two coils is shown in Fig.5 as a function of the field decrease ΔH. The initial slope of the minor hysteresis loop is (-1), equal to the slope in the perfect diamagnetic state. This value can thus be used to calibrate the susceptibility scale of Fig.5.

The critical state model (Eqs.3.9 and 3.10) determines uniquely the flux density profile $B_+(r)$ in the specimen after increasing the applied field monotonously from 0 to H_0 (Fig.6, solid curve). When the applied field is now decreased, at first this profile remains unchanged as long as $|B_+(R) - B_0(H_0-\Delta H)|$ is less than the critical surface discontinuity ΔB_s^c. The corresponding horizontal part of the susceptibility curve in Fig.5 extends from $\Delta H = 0$ to ΔH_0 which is related to ΔB_s^c by

$$\Delta H_0 = 2 \cdot \Delta B_s^c \cdot (\partial B/\partial H)_0^{-1} \qquad (4.3)$$

(Appendix B). A further decrease of the applied field then causes vortices to leave the specimen, and again a critical state will adjust itself ($B_-(r)$, dotted curve of Fig.6). As long as the field decrease ΔH is not too large, i.e. the induction discontinuity can be considered constant, the profile $B_-(r)$ is exactly symmetric to $B_+(r)$. The maximum depth x up to which the flux density has changed is determined by the condition $B_+(R-x) = B_-(R-x)$, the induction at this depth being

$$B_+(R-x) = B_0(H_0) - 0.5 \times (\partial B/\partial H)_0 \cdot \Delta H, \text{ for } \Delta H > \Delta H_0 \quad . \qquad (4.4)$$

As shown in Appendix B, the susceptibility of Fig.5 is given by

$$-\chi = 1 - \frac{P}{\mu_0 A} \cdot (\partial B/\partial H)_0 \cdot x \quad , \qquad (4.5)$$

when the front of the profile change is at depth x (P is the periphery, and A the area of the specimen's cross section).

Equations (4.4) and (4.5) are two linear relations between χ and x on the

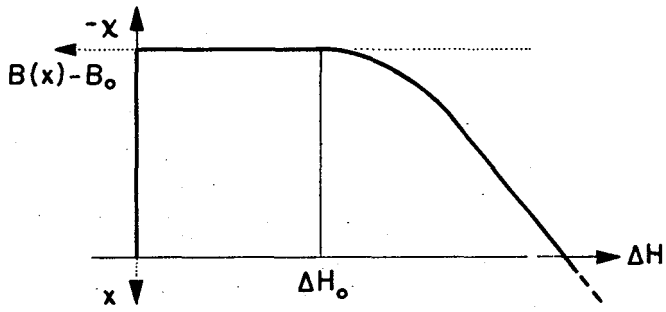

Fig.5 - Differential susceptibility as a function of the field decrease ΔH in the rninor hysteresis loop.

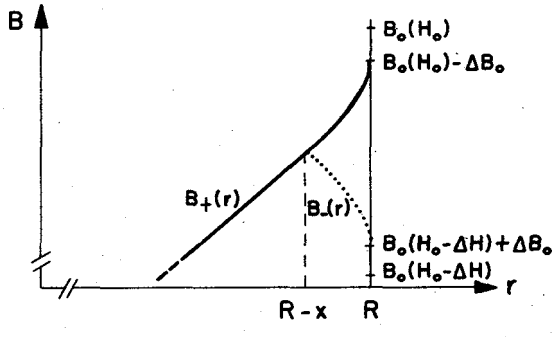

Fig.6 - Flux density profiles $B_+(r)$ and $B_-(r)$ in the specimen during a rninor hysteresis loop (schematic).

one hand, and $B(R-x)$ arid ΔH on the other hand. Thus the susceptibility curves $\chi(\Delta H)$ are immediately linear representations of the profile $B_+(x)-B(H_0)$ near the surface,. turned for 90^0, as indicated by the dotted coordinate system of Fig.5.

Despite this important advantage for the analysis of the measured curves, a.c. methods are frequently preferred because of the increased resolution which, e.g. in the "direct waveform analysis" of Rollins et $al.$[80], is more than an order of magnitude higher (0.2μm) than in the differential susceptibility measurements (± 5μm). Considering the lattice constant of the FLL (0.1 - 0.2 μm in niobium) and the far-reaching mutual interaction of the vortices, however, it might be doubted whether this higher resolution really provides more relevant information and not just incidental microscopic details.

4.2. Field Profiles on Cylinder Faces and in Slits

As the normal component of the magnetic induction $\vec{B}$ is continuous at a surface, the flux profile - outside but very near a plane surface intersecting normally the vortices - is identical to the profile in the interior. Three principally different methods have been developed for the observation of this field profile.

Based on earlier works with a moving Hall probe[82,83], Weber and Riegler measured simultaneously the field in a number of very small Hall probes arranged along a diameter of the sample[S4]. By miniaturization of the probes, a resolution of better than 0.5mm was obtained[85,86]. To decrease the effect of the field distoction in the small gap between sample face and probe, and within the probe thickness, a slit geometry is generally used.

The other two methods can only be applied to an end surface of a specimen. In the technique of Essmann and Träuble[36], the points where the surface is intersected by flux lines are decorated by very small ferromagnetic particles, the whole arrangement then being investigated, by a replica technique, in an electron microscope. This method allows of a direct counting of the vortex densities and shows, furthermore, a lot of details like dislocations in the FLL. However, the technique is highly sophisticated and

time consuming, so its application just to determine flux density gradients in general does not seem to be justified.

A compromise between the complicated high-resolution and the relative simple low-resolution method may be possibly provided by the magneto-optical method[87,89] originally restricted to observations of the coarser domain structure of type-I superconductors in the intermediate state[90], but recently also applied, with promising results, to type-II superconductors[91]. A thin film of a material with high Faraday rotation is evaporated on a specimen surface, and the flux distribution is observed *in situ* by an optical polarization microscope. Because of the use of visible light, it is not possible to resolve individual vortices. However, since differences in the mean flux density cause different angles of rotation of the polarization plane, flux density gradients can be detected. This method seems to be especially appropriate to observe the general geometry of flux entry and rapid flux movements[92].

Although these methods are powerful tools to get much information about flux density profiles, there remains some uncertainty with respect to the edges of the observed surface, Thus they are probably restricted to the determination of the flux distribution in the bulk of the specimens, below a certain surface sheath.

5. EXPERIMENTAL RESULTS

5.1. Flux Density Profiles

The profiles, determined by one of the methods described in the Sections 4.1 or 4.2, generally exhibit the following common characteristics (Fig.7): the flux density gradient in a surface layer of a few μm is extremely high. This is only observable by the described a.c. methods. The other techniques determine this short range drop of the flux density as a discontinuity ΔB_s^c at the surface. After a transition region of up to 200μm, the flux density gradient becomes constant, or, for high gradients, slowly varying with the mean flux density.

In terms of the generalized critical state model as descríbed in Section 3, the flux density gradient α in the interior of the specimen is related to

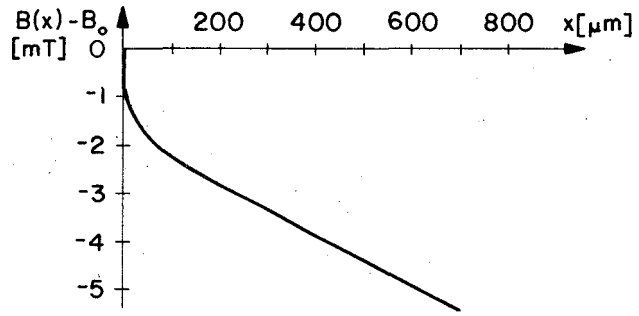

Fig.7 - Typical flux density profile near the surface in increasing field: deviation of the local flux density B from the equilibrium value $B_0(H)$ as a function of the distance x from the specimen's surface (deformed niobium single crystal, B_0 = 180 mT, T = 4.2K, Ref. 93).

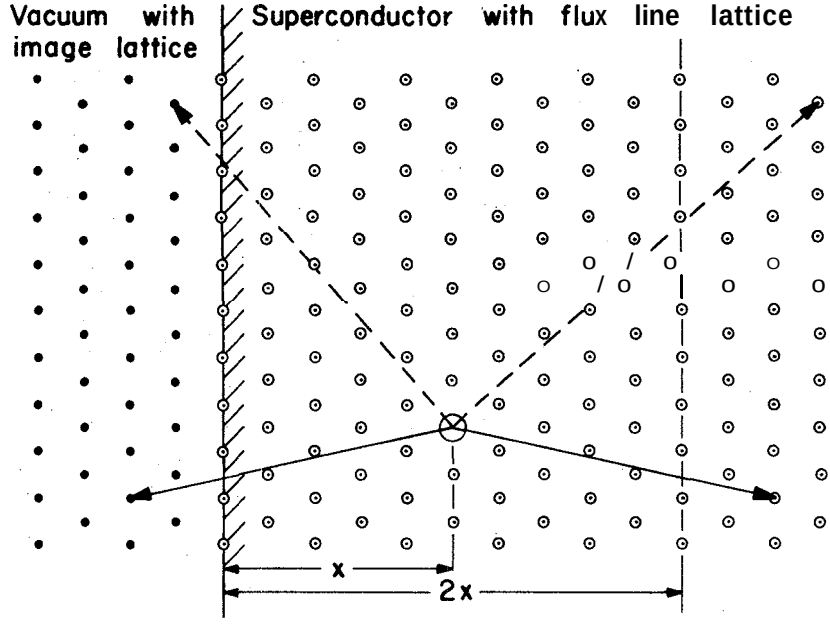

Fig.8 - Flux line lattice and image lattice near the surface.

the mean bulk pinning force, p_v, by eq.(3.5), while the surface discontinuity, ΔB_s^c, is caused by a surface pinning force p_s (Eq.3.8). The existence of a transition region with a curved flux profile up to a distance of sometimes 0.2mm, however, cannot be explained by this model if cylindrical symmetry is assumed. Although it was possible, in a special case, to relate this "near-surface" effect to oxides in a surface layer of niobium[9], this cannot be the only reason because in other experiments it was observed that it varied strongly with the surfaces roughness even for the same oxidation states[61,62].

5.2. Volume Pinning Force

There is a great number of publications describing measurements of flux pinning by different defects in the bulk of specimens. Sometimes, it was possible to relate the measured volume pinning forces quantitatively to the theoretically calculated microscopic interaction, mainly when precipitates are the pinning centers (Refs.68, 95-99). A quantitative investigation of the influence of dislocations, however, is much more difficult[100,101]. This is due to the fact that the dislocation distribution in deformed single crystals, where these measurements are made (Refs. 60, 75, 102-104), is far from being homogeneous, and furthermore is highly anisotropic, whereas the theoretical calculations are mainly restricted to the case of a statistical distribution of dislocations parallel to the vortices.

Qualitatively, it can be said that the pinning force of individual dislocations is rather weak. A quantitative description of the effects of an inhomogeneous dislocation distribution, however, becomes very complicated because of the fact that in these cases besides the long-range stress field of dislocation groups, pile-ups, and networks, a variation of the electron mean free path in regions of high dislocation density may give rise tolocal variations of the Ginzburg-Landau parameter (A-K pinning). Such a combination of elastic and A-K interactions is also responsible for the high critical currents of the technical superconductor NbTi. It is interpreted as arising from precipitates nucleated along dislocations[105,106]. Possibly, a similar effect may be taken advantage of to increase the critical current of A-15 superconductors[107].

For the application of superconducting magnets in future fusion reactors, the influence of radiation damage on the critical current is essential. It is expected that the defects produced by irradiation (interstitial and vacancy dislocations, loops, voids, etc) are effective pinning centers. In pure metals and simple alloys, this was really observed[72]; in systems like Nb_3Sn or Nb_3Ge, however, the resulting decrease of long-range orders, and the corresponding decrease of the critical temperature[108,110] are of much greater influence.

The "scaling laws" first introduced by Fietz and Webb[111], and discussed extensively by Kramer[112], can be used to analyse the underlying interaction mechanism which gives rise to an observed volume pinning force. These scaling laws are based on the fact that the field and temperature dependence of the volume force frequently can be expressed as

$$p_v = C.B_{c2}^{n}.f(B/B_{c2}) \ , \qquad (5.1)$$

where the constants C and n and the function f can be compared with expressions characteristic of each pinning mechanism. The exponent n, which describes the temperature dependence, generally lies between 1 and 3, and the field dependence can frequently be approximated by an expression like

$$f(b) = b^{h}.(1 - b)^{k} \ , \qquad (5.2)$$

with $b = B/B_{c2}$, $0 \leq h \leq 1$, and $1 \leq k \leq 2$.

5.3. Surface Forces

Although the critica1 surface discontinuity ΔB_c^c, or the equivalent surface current, was observed in a number of flux pinning experiments, it was not generally realized that this corresponds to a pinning force. Further systematic investigations, besides the few existing ones, seem to be very important, considering that, on the one hand, the "surface" region of the FLL extends down to a depth of the order of some μm (10 to 20 lattice constants, see Appendix A), and that, on the other hand, the filaments in modern technical composite wires have diameters of 5 - 10μm.

Most of the earlier papers discuss the effect of the surface in terms of an intrinsic surface current related to the surface superconductivity between H_{c2} and H_{c3} (Refs.113,115), or to image forces[57,63]. If these were the only causes, roughening of the surface should decrease the effect. However, the opposite was observed much more frequently, i.e., increase of pinning by roughening of the surface[59,62]. The surface roughness was produced by scratching or grinding, by the slip lines occurring in plastic deformation of single crystals, or by chemical etching. In the first type of measurements, it might be difficult to distinguish the effect of roughness from that of the dislocations produced simultaneously, but the other two experiments seem to be conclusive.

Das Gupta and Kramer[116] observed another effect of the surface: surface pinning varied in the same way as the bulk pinning conditions were altered, even at the same polished surface. They concluded that crystal defects (dislocations in their case) near the surface are much more effective pinning centers than the same species of defect in the bulk. As already mentioned in Section 2, this is probably due to the softening of the elastic constant C_{66} of the FLL near the surface (Appendix A).

All kinds of surface pinning may be reduced considerably by plating the specimen with a magnetic metal or another superconductor. Evetts[117] and Campbell[118] investigated especially the effect of a diffused thallium layer on the surface of specimens of a lead-thallium alloy. They were able to suppress completely surface pinning of unpolished as well as of polished surfaces. The explanation is based, on the one hand, on the altered boundary conditions reducing the effect of the Bean-Livingston barrier [57] as well as of the lattice softening and, on the other hand, the diffusion process reduces also the surface roughness.

5.4. Field History Effects

The critical state model predicts that the critical flux density gradient for a given defect distribution is a unique function of the local flux density and of temperature. The absolute value of the critical gradient should thus be the same on the increasing and on the decreasing branch of an isothermal magnetization curve, and the minor hysteresis loops should be com-

pletely symmetrical. Experiments have shown, however, that both of these requirements are frequently violated (Refs.76, 80, 119), especially in applied fields $H < 0.5\ H_{c2}$, but recently also observed in fields up to $0.9\ H_{c2}$ (Refs.93, 120). Generally, it is found that the critical flux density gradient is lower along the branch of decreasing field. No correlation seems to exist between this field hystory effect and the absolute value of the critical gradient. The experimental results of different authors contradict each other. In the following Section, some possible causes of this effect are discussed.

A second result not consistent with the critical state model is an asymmetry of the minor hysteresis loops, sometimes observed in d.c. measurements. Apparently the sharp change of the flux density gradient (Fig.6) at $r = R\text{-}X$ is rounded off. Eckert and Handstein[76] conclude that flux variations must occur even deeper than x inside the sample. If this is really the case, it is certainly due to effects of nonlocal elasticity. For a complete understanding, also relaxation effects have to be taken into account. De Lima[120] observes this asynunetry only if the field is maintained constant for some seconds after the first semi-cycle, before completing the minor loop (trapezoidal pulses). If both semi-cycles follow each other immediately (triangular pulses), the loops exhibit a nearly perfect symmetry. These measurements were made with a sweep rate of the applied field of 4mT/s.

When the sweep rates are much higher, as they are general1y in a.c. measurements, relaxation effects due to the viscous damping of the oscillating vortices may occur. Bodmer[104] observed, however, that this effect influences the shape of the hysteresis loops only for frequencies of about 60Hz and higher, which corresponds to sweep rates of the order of at least 100 mT/s.

6. DISCUSSION

As outlined by Schmucker[40], the magnetization processes in a cylindrical type-II superconductor are only possible by plastic deformation of the flux line lattice. Here, the reversible part of the minor hysteresis loops may be interpreted as the elastic deforrnation of a surface layer of the

FLL preceding the plastic flow, with the field decrease $\Delta H_0/2$ corresponding to the critica1 shear stress of that surface layer. There are some important differences, however, between the elasto-plastic deformation of a material crystal and a flux line crystal.

In deformation experiments of material crystals, the macroscopic elastic stress is uniform throughout the specimen. When the critical shear stress in the most favorable glide system is reached, plastic deformation begins in the entire volume.

In the case of a FLL, in an irreversible superconductor, pinning centers prevent the elastic stress initially from penetrating farther than into a thin surface layer. Thus, the surface plays a dominant role in the deformation of the FLL. This leads to another important difference. The flow stress in a material crystal is mainly determined by a number of bulk properties: it is the necessary stress to activate dislocations sources or to move dislocations over obstacles (e.g. precipitates or the stress field of other dislocations). Although this type of flow stress also exists inthe FLL (Ref.39), surface effects probably play here a preponderant role. This is due to the fact that, in the case of the FLL, the elasto-plastic continuum itself has to be created or destroyed at the surface, simultaneously with the plastic deformation. Thus, the critica1 shear stress (the possible field decrease ΔH_0 withouth flux change) is mainly determined by surface forces.

The experiments show that there are at least three sources of surface pinning forces:

a. The Bean-Livingston barrier[57] arising from image forces is only relevant at very smooth surfaces of samples with weak bulk pinning, the applied field being exactly parallel to the surface. Otherwise, it is masked by the much stronger contributions b. or c.

b. Because of the softening of the elastic shear constant C_{66}, pinning centers like precipitates or dislocations are much more effective near the surface than in the bulk (Section 2.3 and Appendix A).

c. There is a direct interaction of the vortices with the asperities of a rough surface.

Only qualitative suggestions for the origin of this latter interaction exist

at the moment. One contribution should arise from the length variation of the part of a vortex within a surface asperity. The extreme case of this mechanism, vortices crossing perpendicularly a surface of well-defined roughness, was investigated experimentally by Morrison and Rose[121].

A second contribution to the observed pinning of a rough surface may be due to the necessarily numerous initial intersections of a flux line with the surface asperities. At each intersection, the vortex is strongly distorted[122]: which increases its self-energy. If the vortex it not normal to the intersected surface, this energy is further increased by a curvature of the line.

The depth of the layer where these mechanisms are effective is less than 2µm, in many cases only about 0.5µm. Thus, they are no doubt responsible for the discontinuity ΔB_s of the flux density in the surface, but they are not able to explain the observed enhanced flux density gradient in adepth of up to 200µm (Fig.7, transition region). To understand this observation, we proposed some ideas[62] which are based on the flux spot model of Hart and Swartz[59].

The critica1 state as described thus far is a two-dimensional model, assuming straight flux lines in an infinite parallel cylinder. In reality, however, the flux line will not penetrate into the cylinder at once over its entire length. Initially, it will be created over a short length only at such a point of the surface where the nucleation energy is occasionally lowered (e.g. near the end faces or at other geometric or chemical inhomogeneities). During the further flux penetration, the points of exit of this flux line have to move longitudinally along the cylinder surface ("flux spots"). Even when the center section of a line is already in the bulk of the specimen (e.g. 200µm deep), one or both end sections of the same line are still in the surface layer, where they are subject to the high surface forces. Because of the line tension of the vortices, the deeper penetrated parts of the line are coupled elastically to these end sections, thus still feeling, although indirectly, the surface forces. This mechanism wi11 be even more pronouced if the surface is not exactly parallel to the applied field.

In samples with a strong anisotropy of the macroscopic pinning forces (e.

g., plastically deformed single crystals), there is another mechanism leading to an apparent deep reaching enhanced flux density gradient. The induced voltage in the pick-up coil is an integrated signal over all azimuthal directions. The analysis of the curves by Eqs.(4.4) and (4.5) thus yields mean values of the eventually anisitropic flux density gradients. If the anisotropy is however so strong that the flux changes in some directions have penetrated into the bulk region whilst, in other directions, they have not yet overcome the surface layer, the susceptibility method yields an averaged value between surface and bulk properties without much significance, simulating an enhanced gradient in a layer much thicker than it is in reality.

The influence of the magnetic field history, the fact that the absolute value of the flux density gradient is different in increasing and decreasing field, is hardly understood yet. One of the properties which mightbe different on the two branches of the magnetization curves is the density and distribution of dislocations in the FLL (Ref.119). If there are no Frank-Read sources[123] in the bulk of the FLL, all dislocations have to be created at the surface. In an increasing field, they will originate and penetrate into the bulk together with the vortices. In a decreasing field, however, the flux line lattice arises at first homogeneously in the whole cross section as soon as the field reaches H_{c2}. The dislocation density of this initial high-field lattice is probably rather low. When the field is now decreased, the necessary dislocations to build up a flux density gradient have to be created at the surface and penetrate deep into the bulk opposite to the direction of flux movement. This will in general result in another dislocation density and distribution rather than in an increasing field.

At first sigkt, this mechanism should give rise to the strongest field history effect at fields just below H_{c2}, where the difference in the dislocation density between increasing and decreasing field is greatest, in contradiction to all observations. At these high fields, however, the shear modulus of the flux line lattice is so small[28,24] that it behaves more like a "liquid" than like a "solid", without the necessity of dislocations for a plastic shear.

Another mechanism whích may contríbute to the field history effect is ba-

sed on the surface barrier of a rough surface. If this barrier is very much stronger for leaving, than for entering, vortices, it may become possible that in decreasing field some sectors of a cross section are pinned completely by the surface. In minor hysteresis loops, these sectors will not contribute to the total flux change which therefore is less than expected from the gradient. The averaging measurement thus sirnulates a lower flux density gradient in decreasing field.

Similar mechanisms may contribute to the observed asymmetry of the rninor hysteresis loops. Besides this, the nonlocality of the elasticity of the flux line lattice will play an important role here. The Friedel force on an element of the FLL is then determined not only by the local flux density gradient, as described by Eq. (3.5), but also by the gradients in the vicinity, up to a distance of severa1 lattice constants[24]. In the model calculations of Section 4 and Appendix B, it was assumed that the critical state is always realized by a constant flux density gradient. By the nonlocal elasticity of the flux line lattice, this cannot be completely true in minor hysteresis loops near $r=R-x$ (Fig.6), where the flux density gradient suddenly would change its sign. Detailed calculations[120] show that, during the formation of the flux profile in minor hysteresis loops (Fig.6), a generalized Friedel force acts in the direction of the sample surface even at a radius slightly less than (R-x). This gives rise to a blunting of the sharp edge in the flux density profile, at $r=R-x$, as observed by Eckert and Handstein[76].

In minor hysteresis loops, relaxation processes frequently cannot be neglected. At least two relaxation times have been observed. The first is of the order of 10ms; this is probably due to viscous damping of the vortices, and only becomes important for a.c. measurements with higher frequencies[104]. The second relaxation time is of the order of 1s; it describes the flux creep or "settling down" of the flux profile immediately after it was forced to change. This relaxation time is consistent with the results of direct flux creep measurements in hollow cylinder[68] or by a SQUID technique[69].

APPENDIX A: SOFTENING OF THE FLUX LINE LATTICE NEAR A SURFACE

The pair interaction potential between two parallel London flux lines at a distance r is given by

$$U(r) = 2(\phi_0/4\pi\lambda)^2 K_0(r/\lambda) \quad , \tag{A.1}$$

where $K_0(x)$ is the modified Bessel function, and λ the penetration depth. Calling J the self energy of a flux line, the total energy of an arbitrary arrangement of N flux lines can be written as[29]

$$F = N.J + \sum_{i<j} U_{ij} \quad , \tag{A.2}$$

as long as all mutual distances are large compared with core dirnensions. Following Brandt[29], the bulk modulus C_L is given by

$$C_L = \frac{\Delta F}{V} \cdot \frac{1}{2\varepsilon^2} \quad , \tag{A.3}$$

with the strains $\varepsilon_{xx} = \varepsilon_{YY} = \varepsilon$, and the shear constant C_{66} by

$$C_{66} = \frac{\Delta F}{V} \cdot \frac{1}{\alpha^2} \quad , \tag{A.4}$$

with the shear angle $\alpha = \varepsilon_{xy} + \varepsilon_{yx}$. The two constants can be calculated by deforming the lattice homogeneously and calculating the corresponding variations ΔF of the total energy (A.2).

Eqs. (A.3) and (A.4) are only useful if C_L and C_{66} are constant within the volume V. To use them also for the calculation of possibly varying constants, we choose for the volume one lattice cell and substitute the double sum in ΔF by a single sum over the variations in the pair potentials ofone flux line. Taking account of the lattice symmetries this leads finally to the expressions[29]

$$C_L = \frac{n}{8} \sum_{\mu} \frac{d^2U(r_\mu)}{dr_\mu^2} \cdot r_\mu^2 \quad , \tag{A.5}$$

$$C_{66} = \frac{n}{16} \sum_{\mu} \left[\frac{d^2U(r_\mu)}{dr_\mu^2} + \frac{3}{r_\mu} \cdot \frac{dU(r_\mu)}{dr_\mu} \right] \cdot r_\mu^2 \quad . \tag{A.6}$$

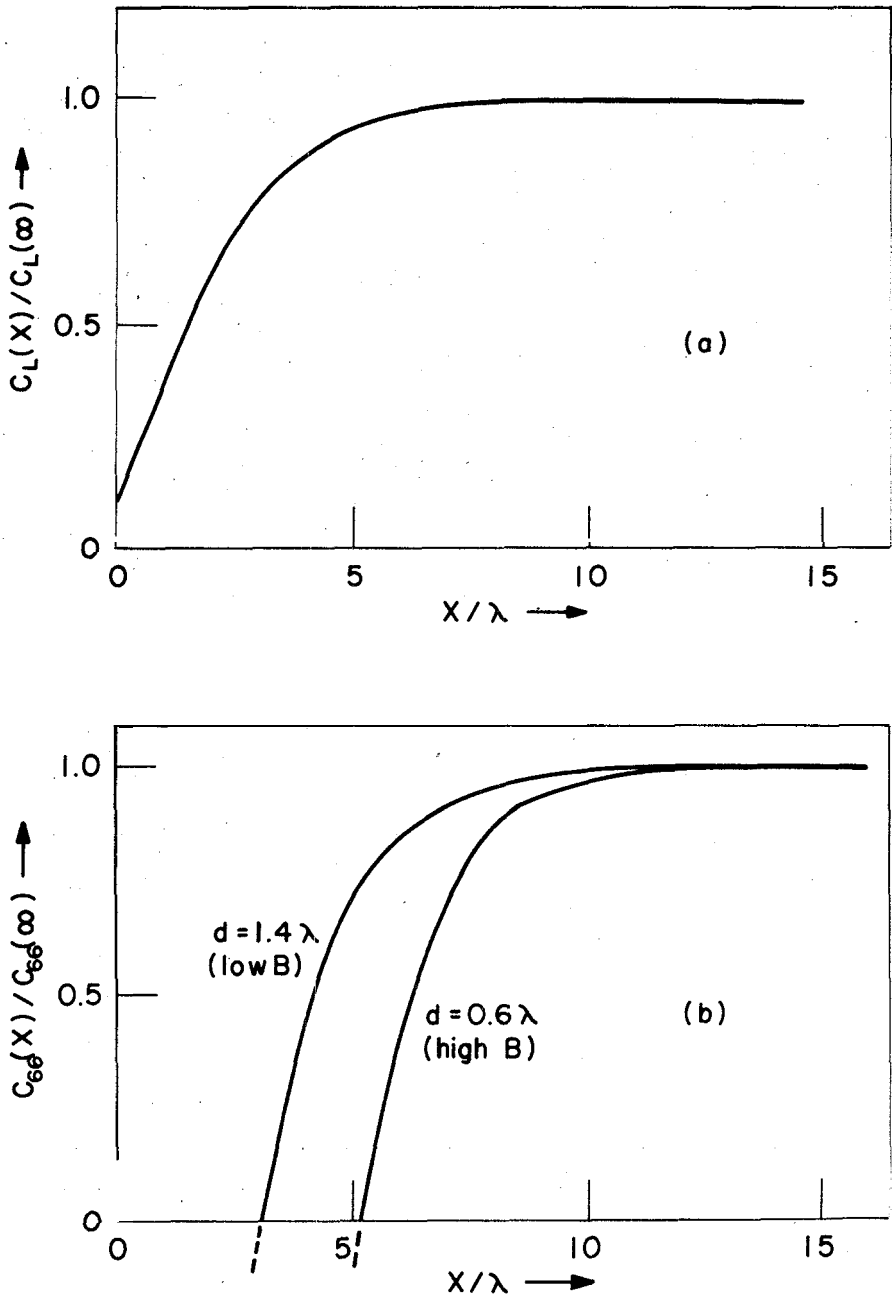

Fig. 9 - Softening of the elastic constants C_L and C_{66} of the FLL near a plane surface.

Considering a flux line at a distance x from a parallel plane surface, outside of which there is vacuum with a lattice of image lines (Fig.8), all contributions to the sums in Eqs.(A.5) and (A.6) coming from flux lines deeper than $2x$, within the sample, are cancelled by the contributions of the image lines. Numerical summation becomes thus very simple and yields the dependence of the elastic constants shown in Fig.9a and b: Both constants decrease considerably near the surface, especially the shear constant C_{66}, the softening of which already begins in a depth of 10 to 12 λ ($\sim$0.5μm in the case of Nb). The naive application of Eqs.(A.5) and (A.6), for a regular FLL up to the surface, would even give negative shear constants very near the surface. In reality this means that in this region the vortices form a "flux line liquid" rather than a flux line lattice.

APPENDIX B: DIFFERENTIAL SUSCEPTIBILITY IN MINOR HYSTERESIS LOOPS

The flux density profile, $B_+(r)$, after increasing the applied field monotonously from 0 to H can be calculated from Eqs. (3.9) and (3.10):

$$B_+(r) = B_0(H_0) - \Delta B_s^c - \int_r^R \alpha \, . \, dr' \quad . \tag{B.1}$$

Decreasing now the applied field, this profile will not change until $\Delta H = \Delta H_0$, where ΔH_0 is determined again by Eq. (3.10), now with the opposite sign, i.e.

$$B_0(H_0 - \Delta H_0) + \Delta B_s^c = B_0(H_0) - \Delta B_s^c \quad , \tag{B.2}$$

which yields, for ΔB_s^c, the critical flux density discontinuity in the surface:

$$\Delta B_s^c [B_+(R)] = \frac{1}{2}\left[B_0(H_0) - B_0(H_0 - \Delta H_0)\right] = \frac{1}{2}\,(\partial B/\partial H)_0 \, . \, \Delta H_0 \quad . \tag{B.3}$$

For $\Delta H > \Delta H_0$, flux lines leave the sample, and the new critical state is given by the profile $B_-(r)$:

$$B_-(r) = \begin{cases} B_0(H_0-\Delta H) + \Delta B_s^c + \int_r^R \alpha . dr' \text{ , for } R-x \leq r \leq R \text{ ,} \\ B_+(r) \text{ , for } r \leq R-x \text{ .} \end{cases} \quad (B.4)$$

The flux density varies down to the depth x, given by the condition $B_-(R-x) = B_+(R-x)$, and thus related to the field decrease ΔH by

$$\int_{R-x}^{R} \alpha . dr' = \frac{1}{2} \left[B_0(H_0-\Delta H_0) - B_0(H-\Delta H)\right] = \frac{1}{2} (\partial B/\partial H)_0 . (\Delta H - \Delta H_0) \text{ ,} \quad (B.5)$$

so that the flux density, at $R-x$, becomes

$$B(R-x) = B_0(H_0) - \frac{1}{2} (\partial B/\partial H)_0 . \Delta H \text{ .} \quad (B.6)$$

The total decrease of the magnetic flux in the sample is

$$\Delta\phi = \int_A \left[B_-(r) - B_+(r)\right] dr \text{ ,} \quad (B.7)$$

which can be approxirnated by

$$\Delta\phi = P \cdot \int_{R-x}^{R} \left[B_-(r) - B_+(r)\right] dr \text{ ,} \quad (B.8)$$

if $x \ll R$, where P is the periphery of the cross section A. With the relations $\overline{\Delta B} = \Delta\phi/A$ and $H_a = H - \Delta H$, the differential susceptibility $\chi = d\bar{M}/dH_a$ becomes

$$-\chi = 1 - \frac{1}{\mu_0 A} \cdot \frac{d\Delta\phi}{d\Delta H} \text{ ,} \quad (B.9)$$

which cornbined with (B.4), (B.5), and (B.8), takes the form

$$-\chi = 1 - \frac{P}{\mu_0 A} (\partial B/\partial H)_0 \, x \quad (B.10)$$

The linearity of Eq. (B.IO) is a direct consequence of the condition $x \ll R$. For a circular cross section, however, it is possible to generalize this equation in order to make it valid for the whole cross section:

$$-\chi = 1-(2/\mu_0)-(\partial B/\partial H)_0 . (x/R) . [1-(x/2R)] . \qquad (B.10a)$$

I thank my colleagues of the low-temperature group of UNICAMP for many helpful discussions. We are especially grateful to Professor D. G. Pinatti, O.F. de Lima, A. S. Brito and M. S. Torikachvili for their valuable contributions. My particular gratitude is due to Dr. U. Essmann and Dr. A. Bodmer, Stuttgart, for their careful reading of the manuscript and for many important suggestions, as well as to Dr. B. M. Kale for correcting the worst language errors.

Part of the experiments described in this article were supported by FAPESP.

BIBLIOGRAPHY

a. General textbooks on superconductivity

1. E.A. Lynton, *Superconductivity* (Chapman and Hall, London, 1969).
2. P.G. de Gennes, *Superconductivity of Metals and Alloys* (w.A. Benjamin, New York, 1966).
3. R.D. Parks, ed., *Superconductivity* (Marcel Dekker, New York, 1969).
4. S. Saint-James, G. Sarma and E. J. Thomas, *Type-II Superconductivity* (Pergamon Press, Oxford, 1969).
5. A.C. Rose-Innes and E.H. Rhoderick, *Introduction to Superconductivity* (Pergamon Press, Oxford, 1969).

b. Books and review articles about selected topics

6. H. Brechna, *Superconducting Magnet Systems* (Springer-Verlag, New York, Heidelberg, Berlin, 1973).
7. B.B. Schwartz and S. Foner, *Large-scale Application of Superconductivity*, Physics Today *30*, 34 (1977).

8. A.M. Campbell and J.E. Evetts, *Critical Currents in Superconductors* (Taylor and Francis Monographs on Physics, London 1972; reprinted from Adv. Phys. 21, 199 (1972)).

9. H. Ullmaier, *Irreversible Properties of Type-II Superconductors* (Springer Tractsin Modern Physics No.76, Springer-Verlag, Berlin, Heidelberg, New York, 1975).

10. H. Freyhardt and P. liaasen, eds., *Proceedings of the International Discussion Meeting on Flux Pinning in Superconductors* (Sonnenberg, West Germany , 1975).

11. P.H. Melville, *A.C. Loss and Related Effects in Type-11 Superconductors*, Adv.Phys. 21, 647 (1972).

12. J.D. Livingston and H.W. Schadler, *The Effect of Metallurgical Variabtes on Superconducting Properties*, Progr. in Mat. Sci. *12*, 183 (1964).

c. Original research papers

13. J.E. Kunzler, E. Buehler, F.S.L. Hsua and J.H. Wernick, Phys. Rev. Lett. *6*, 89 (1961).

14. Y. Kyotani, Cryogenics 15, 372 (1975).

15. E.B. Forsyth, Cryogenics *17*, 3 (1977).

16. C.P. Bean, Phys. Rev. Lett. 8, 250 (1962).

17. V.L. Ginzburg and L.D. Landau, Zh. Eksperim. i Teor. Fiz. *20*, 1064 (1950).

18. B.B. Goodman, IBM J. Res. Dev. 6, 63 (1962).

19. A.A. Abrikosov, Zh. Eksperim. i Teor. Fiz. *32*, 1442 (1957).

20. D. Cribier, B. Jacrot, L. Madhov Rao and B. Farnoux, Phys. Lett. 9, 106 (1964).

21. H. Träuble and U. Essmann, Phys. Stat. Sol. 18, 813 (1966).

22. U. Essmann and H. Träuble, Phys. Lett. *24A*, 526 (1967).

23. J. Schelten, H. Ullmaier and G. Lippmann, Z. Physik 253, 219 (1972).

24. E.H. Brandt, J. Low Temp. Phys. 26, 709 (1977).

25. E.H. Brandt, J. Low Temp. Phys. 26, 735 (1977).

26. V.G. Kogan, J. Low Temp. Phys. 26, 953 (1977).

27. R. Labusch, Phys. Stat. Sol. 19, 715 (1967).

28. R. Labusch, Phys. Stat. Sol. 32, 439 (1969).

29. E.H. Brandt, Phys. Stat. Sol. 35, 1027 (1969).

30. E.H. Brandt, Phys. Stat. Sol. *36*, 381 (1969).

31. G. Zerweck, Phys. Stat. Sol. (b) 78, K 15 (1976).

32. E.H. Brandt, Comm. on Phys. 1, 57 (1976).
33. R. Schmucker and E.H. Brandt, Phys. Stat. Sol. (b) 79, 479 (1977).
34. E.H. Brandt, Phys. Stat. Sol. (b) 77, 551 (1976).
35. R. Labusch, Phys. Lett. 22, 9 (1966).
36. H. Träuble and U. Essmann, J. Appl. Phys. 39, 4052 (1968).
37. J.A. Good and E.J. Kramer, Phil. Mag. 24, 339 (1971).
38. U. Essmann and R. Schmucker, Phys. Stat. Sol. (b) *64*, 605 (1974).
39. R. Schmucker, Phil. Mag. 35, 431 (1977).
40. R. Schmucker, Phil. Mag. *35*, 453 (1977).
41. R. Schmucker, Phys. Stat. Sol. (b) 80, 89 (1977).
42. E. Kröner, *Kontinuumstheorie der Versetzungen und Eigenspannungen* (Springer-Verlag Berlin, Göttingen, Heildelberg, 1958).
43. E.J. Kramer and C.L. Bauer, Phil. Mag. *15*, 1189 (1967).
44. H. Kronmüller and R. Schmucker, Phys. Stat. Sol. (b) 57, 667 (1973).
45. R. Schmucker and H. Kronmüller, Phys. Stat. Sol. (b) 61, 181 (1974).
46. W.W. Webb, Phys. Rev. Lett. *11*, 191 (1963).
47. A. Seeger and H. Kronmüller, Phys. Stat. Sol. (b) 27, 371 (1968).
48. H. Kronmüller and A. Seeger, Phys. Stat. Sol. (b) 34, 781 (1969).
49. E. Schneider, *Dissertation* (University of Stuttgart, 1976).
50. E. Schneider and H. Kronmüller, Phys. Stat. Sol. (b)*74*, 261 (1976).
51. H. Teichler, Phys. Stat. Sol. (b) 69, 501 (1975).
52. K. Yamafuji and F. Irie, Phys. Lett. *25A*, 387 (1967).
53. F. Irie, K. Yamafuji, J. Phys. Soc. Jap. 23, 255 (1967).
54. R. Labusch, Cryst. Latt. Def. *1*, 1 (1969).
55. G. Kornfeld and H. Kronmüller, Phys. Stat. Sol. (b) 44, 647 (1971).
56. P. W. Anderson, Phys. Rev. Lett. 9, 309 (1962).
57. C.P. Bean, J.D. Livingston, Phys. Rev. Lett. 12, 16 (1964).
58. J.R. Clem, R.P. Huebener and D.E. Gallus, J. Low Temp. Phys. 12, 449 (1973).
59. H. R. Hart and P. S. Swartz, Phys. Rev. 156, 403 (1967).
60. G. Zerweck, Phil. Mag. 27, 197 (1973).
61. A. S. Brito, *Tese de Mestrado* (State University of Campinas, 1977).
62. A.S. Brito and G. Zerweck, to be published.
63. J. Lowell, J. Phys. *C2*, 372 (1969).
64. E. J. Kramer and A. Das Gupta, Phil. Mag. 26, 769 (1972).
65. J. Friedel, P.G. de Gennes and J. Matricon, Appl. Phys. Lett. 2, 119 (1963).

66. J. E. Evetts and A. M. Campbell, Proc. *of the Tenth Intern. Conf. Low Temp. Phys.*, Vol. IIB, p.33 (Moscow, 1966).
67. D.M. Kroeger and J. Schelten, J. Low. Temp. Phys. 25, 369 (1976).
68. G. Antesberger and H. Ullmaier, Phil. Mag. 29, 1101 (1974).
69. A. Bodmer, H. Gessinger and W. Ludwig, Ref. 10, p. 176.
70. U. Essmann and H. Träuble, Phys. Stat. Sol. 32, 337 (1969).
71. J. Schelten and G. Lippmann, Phil. Mag. 33, 475 (1976).
72. E.L. Andronikashvili, S.M. Ashimov and J.S. Tsakadze, Phys. Stat. Sol. (b) *56*, 79 (1973).
73. H. Ullmaier, K. Papastaikoudis, S. Takacs and W. Schilling, Phys.Stat. Sol. 41, 671 (1970).
74. H. Freyhardt and P. Haasen, Z. Metallk. 58, 856 (1967).
75. H. Freyhardt, Z. Metallk. 60, 409 (1969).
76. D. Eckert and A. Handstein, Phys. Stat. Sol. (a) 37, 171 (1976).
77. C.P. Bean, Rev. Mod. Phys. *36*, 31 (1964).
78. D.M. Kroeger, C.C. Koch and W.A. Coghan, J. Appl. Phys. *44*, 2391 (1973).
79. H. Uilmaier, Phys. Stat. Sol. 17, 631 (1966).
80. R. W. Rollins, H. Küpfer and W. Gey, J. Appl. Phys. 45, 5392 (1974).
81. A.M. Campbell, J. Phys. *C2*, 1492 (1969).
82. H.E. Cline, R.M. Rose and J. Wulff, J. Appl. Phys. 37, 1 (1968).
83. H. Voigt, Z. Physik *213*, 119 (1968).
84. H. W. Weber and R. Riegler, Sol. St. Comm. *12*, 121 (1973).
85. H.W. Weber, G.P. Westphal and I. Adaktylos, Cryogenics *16*, 39 (1976).
86. I. Adaktylos, E. Schachinger and H.W. Weber, J. Low Temp. Phys. *26*, 533 (1977).
87. W. de Sorbo, Cryogenics 4, 257 (1964).
88. H. Kirchner, Phys. Stat. Sol. (a) 4, 531 (1971).
89. H. Kirchner, Rev. Sci. Instr. 44, 379 (1973).
90. A. Kiendl and H. Kirchner, J. Low. Temp. Phys. 24, 349 (1974).
91. H.U. Habermaier and H. Kronmüller, Appl. Phys. 12, 297 (1977).
92. R.B. Harrison, J.P. Pendrys and L.S. Wright, J. Low Temp. Phys. 18, 113 (1975).
93. O.F. de Lima, *Tese de Mestrado* (State University of Campinas, 1977).
94. A. Das Gupta, W. Gey, J. Halbritter, H. Küpfer and J.A. Yasaitis, J. Appl. Phys. *47*, 2146 (1976).
95. A.M. Campbell, J.E. Evetts and D. Dew Hughes, Phil. Mag. 28, 313(1968).
96. R.I. Coote, J.E. Evetts and A.M. Campbell, Can. J. Phys. 50, 421(1972).

97. G. Antesberger and H. Ullmaier, Phys. Rev. Lett.35, 59 (1975).
98. R. Riegler and H.W. Weber, J. Low. Temp. Phys. 15, 431 (1974).
99. H.C. Freyhardt, Phil. Mag. 23, 369 (1971).
100. G.J. Van Gurp and D.J. Van Ooijen, J. Phys. C27, 3 (1966).
101. D. Dew Hughes, and M.J. Witcomb, Phil. Mag. 26, 73 (1972).
102. J.A. Good and E.J. Kramer, Phil. Mag. 22, 329 (1970).
103. H.C. Freyhardt, Phil. Mag. 23, 345 (1971).
104. A. Bodmer, *Dissertation* (University of Stuttgart, 1976).
105. I. Pfeiffer and H. Hillmann, Acta Met. 16, 1429 (1968).
106. U. Zwicker, R. Lohberg and W. Heller, Z. Metallk. 62, 836 (1970).
107. U. Essmann, H. Haag and G. Zerweck, submitted to Comm. on Phys.
108. A.R. Sweedler, D.E. Cox, S. Moehlecke, R.H. Jones, L.R. Newkirk and F. A. Valencia, J. Low. Temp. Phys. 24, 645 (1976).
109. A.R. Sweedler, D. G. Schweitzer and G. W. Webb, Phys. Rev. Lett.33, 168 (1974).
110. M. Fähnle and H. Kronmüller, Comm. on Phys. *1*, 91 (1976).
111. W.A. Fietz and W.W. Webb, Phys. Rev. 178, 657 (1969).
112. E.J. Kramer, J. Appl. Phys. 44, 1360 (1973).
113. R.W. Rollins and J. Silcox, Phys. Rev. 255, 404 (1967).
114. J.G. Park, Adv. Phys. 18, 103 (1969).
115. D. Saint-James and P.G. de Gennes, Phys. Lett. 7, 306 (1963).
116. A. Das Gupta and E.J. Kramer, Phil. Mag. 26, 779 (1972).
117. J.E. Evetts, Phys. Rev. *B* 2, 95 (1970).
118. A.M. Campbell, Phil. Mag. 32, 1191 (1975).
119. L.M. Schafe, P.L. Rossiter and W.A. Rachinger, Phys. Stat. Sol. (b) 74, 785 (1976).
120. O.F. de Lima and G. Zerweck, to be published.
121. D.D. Morrison and R.M. Rose, J. Appl. Phys. 42, 2322 (1971).
122. J. Pearl, J. Appl. Phys. 37, 4139 (1966).
123. F.C. Frank and W.T. Read, Phys. Rev. 79, 722 (1950).